Operational Quantum Gravity: Four Consequences of a Matter-First Response

Todd J. Desiato

Independent researcher, Statesville, North Carolina, USA
Correspondence: mainengineering@gmail.com
ORCID: 0000-0002-7514-0169

Abstract. A completed quantum matter response can support the long-wavelength relations conventionally described by geometry. Operational Quantum Gravity (OQG) begins with the normalized, fixed-measure Standard-Model stress functional, inverts its Ward- and contact-completed response on the physical subspace, and represents its massless two-helicity branch by an Einstein-equivalent Weyl-transverse-diffeomorphism theory. Four consequences are assembled with their distinct premises. An arbitrary homogeneous identity-operator energy shift leaves every local response vertex invariant, removing the radiative local-source vacuum catastrophe. A state-dependent clock and ruler history reconstructs observed cosmic acceleration without a physical dark-energy fluid on a selected zero-integration-datum branch; a quadratic effective-time law fitted to 32 chronometers also describes six DESI DR2 Alcock–Paczyński measurements without refitting. Regular canonical dilation excludes exact zero material extension, with a finite-loading continuation criterion for collapse. Finally, the conserved-source response produces the coherent four-branch gravity-induced entangling phase without a fundamental Einstein–Rosen bridge. The paper distinguishes exact invariance, observational reconstruction, a conditional material-state theorem, and an operational-equivalence result while retaining the tested infrared gravitational equations.

Keywords: operational quantum gravity; vacuum energy; cosmology; black-hole endpoints; gravity-induced entanglement

1. Introduction

A distant galaxy supplies a spectrum measured by matter-built clocks; a black hole is inferred from matter and radiation; and an entanglement experiment records correlations between material probes. The standard geometric descriptions of these observations are powerful. Operational Quantum Gravity (OQG) asks which physical response makes those descriptions work. Its order is a prepared quantum matter state, a completed causal stress response, a constitutive compliance, comparisons by material clocks and rulers, and only then an infrared geometry. This paper assembles that order and its consequences from the versioned derivation and companion manuscripts [1–5]. Fig. 1 records the chain.

Four longstanding questions provide a compact cross-domain test. A *vacuum catastrophe* here means the proposed local gravitational sourcing of an arbitrary radiative identity-operator offset, not every physical effect associated with a vacuum. *Dark energy* means an additional homogeneous substance invoked to produce the observed background acceleration; the conventional fitted kinematic history remains measurable. A *zero-extension endpoint* means a normal material state in which every resolved internal

position-like width vanishes; it is distinct from a horizon or a coordinate limit. An *Einstein–Rosen (ER) bridge* means a literal spacetime tunnel invoked as the structure behind Einstein–Podolsky–Rosen (EPR) correlations. The final application is the Bose–Marletto–Vedral (BMV) gravity-induced-entanglement protocol [6, 7].

The four outcomes have different logical strength. Source-level fixed-measure invariance is an exact functional identity. The cosmic acceleration result is a fitted, reproducible background reconstruction. The collapse result is a state-space theorem with explicit regularity conditions for physical continuation. The BMV result is equality of the coherent infrared phase for conserved sources on a specified causal branch. Table 1 makes the premises and observational discriminators visible before the calculations.

This synthesis has a direct space-science use. Photons from distant sources carry cross-epoch frequency comparisons; cosmic chronometers and baryon-acoustic-oscillation surveys constrain their history. Black-hole observations infer causal structure through matter and radiation outside a horizon. Proposed tabletop entanglement tests ask which part of that gravitational description must itself be quantum. A single operational language keeps measured quantities and physical assumptions attached to each subject. The detailed perturbative, numerical and operator proofs remain in the versioned companion manuscripts [1–5]; the necessary mathematical links appear here.

Table 1. Four results, premises and next discriminators.

Outcome	Additional premise and present result	Independent discriminator
Vacuum-energy zero	Fixed source measure: exact invariance under a common identity shift	Source-dependent polarization, boundary stresses and branch datum remain measurable
Cosmic acceleration	Zero invariant cosmological branch and common epoch standard: chronometer reconstruction with DESI no-refit comparison	Covariance-complete likelihood, structure and early-time probes, microscopic rate
Collapse endpoint	Regular finite canonical sector: no normal exact zero extension; finite loading under an integrable response	High-density scale susceptibility and survival or matching of the branch
Entanglement	Causal two-helicity conserved-source completion: BMV coherent phase and ideal concurrence	Retardation, visibility, correlated noise and higher connected response



Fig. 1. Prepared Standard-Model matter supplies the response; the geometry is its infrared representation. Each outcome also has a premise stated in the text.

OQG's static transverse-traceless (TT) coefficient, causal propagating branch and constrained Newtonian exchange are separate steps. Each is retained below. The static coefficient supplies the residue normalization, while the full frequency-dependent kernel supplies the causal test and the Einstein-equivalent conserved-source completion supplies the finite-body interaction. Three defined physical inputs in the high-state coefficient ledger are the renormalized Higgs–curvature coupling and two three-dimensional Yang–Mills lattice observables. An absolute comparison with Newton's constant also fixes the reference-state intercept. The latter is a normalization datum separate from the three coefficient inputs [1, 2].

2. One normalized source and its long-wavelength representation

The source is a diagnostic coupling to the interacting Standard Model (SM), rather than a second microscopic system. Let $q_{+\mu\nu}$ and $q_{-\mu\nu}$ be independent symmetric tensor sources on the forward and backward branches of a closed-time-path (CTP) history. Let $T_{+}^{\mu\nu}$ and $T_{-}^{\mu\nu}$ be the corresponding complete SM stress tensors. The source convention is [1]

$$S_{src}^{CTP}=\frac{1}{2}\int d^4x\left(q_{+\mu\nu}T_{+}^{\mu\nu}-q_{-\mu\nu}T_{-}^{\mu\nu}\right). \quad (1)$$

With a normalized prepared density operator ρ_i, an SM evolution operator U_q in the source history q, and the trace over matter states denoted by Tr, define

$$Z\left[q_{+},q_{-}\right]=Tr\left(U_{q_{+}}\rho_i U_{q_{-}}^{\dagger}\right), W\left[q_{+},q_{-}\right]=-i\ln Z\left[q_{+},q_{-}\right], Z\left[q,q\right]=1. \quad (2)$$

The average source is $q_r=\left(q_{+}+q_{-}\right)/2$, and the difference source is $q_a=q_{+}-q_{-}$. Equal sources are imposed after variation. Capital labels A, B abbreviate symmetric tensor-index pairs and their spacetime arguments. The physical retarded susceptibility is the response of the mean stress to the average source,

$$\Pi_{AB}^{R}(x,y)=2\frac{\delta^2 W}{\delta q_{a,A}(x)\delta q_{r,B}(y)}\bigg|_{q_a=0}=-\frac{i}{2}\theta\left(x^0-y^0\right)\left\langle\left[T_A(x),T_B(y)\right]\right\rangle+\Pi_{AB}^{R,contact}(x,y). \quad (3)$$

Here θ is the causal step function. The contact term is generated because the full stress operator itself varies with the source. Keeping that term completes the Ward identity before inversion. Gauge and conservation directions are null; inversion is performed only on the nonsingular physical subspace. The static TT Euclidean susceptibility gives a two-

derivative stiffness $A_{2,E}^{tot}$, including its declared reference state and the calculated state increment. At small Euclidean four-momentum p, its physical block has [1, 2]

$$K_{TT,E}(p)=A_{2,E}^{tot}p^2+O(p^4),D_{TT,E}(p)=(K_{TT,E}(p))^{-1}=\frac{1}{A_{2,E}^{tot}p^2}+O(p^0).(4)$$

The displayed inverse gives a long-range static compliance. The completed high-state stiffness through second order in the SM couplings includes the free, screened, strict-hard, electric/Higgs, local-curvature and magnetostatic terms. The two nonperturbative magnetostatic coefficients and the Higgs–curvature coupling are explicitly defined inputs. The calculation determines state increments; an absolute total uses its reference-state intercept. Equation (4) by itself does not assign a Lorentzian wave speed or a Newtonian force.

In the symmetric-phase benchmark, let $\Theta=k_BT$, where k_B is Boltzmann's constant and T the state temperature. Let ξ_H denote the renormalized Higgs–curvature coupling, and let c_3^{NP} and c_2^{NP} denote the finite matched SU(3) and SU(2) three-dimensional Yang–Mills shear responses. The complete source-normalized state-increment ledger through the stated coupling order is [1]

$$\frac{A_{2,E}^{\Delta}}{\Theta^2}=0.260056206678+0.066624158194\,\xi_H+0.002999279576\,c_3^{NP}+0.000799379974\,c_2^{NP}.(5)$$

These coefficients audit a declared high-state benchmark and matching scheme; they are neither a fit of Newton's constant nor a temperature law for a compact laboratory specimen. The Yang–Mills inputs are finite shear slopes with a prescribed continuum and lattice matching operation, including the source-contact completion. The renormalized Higgs coupling is a distinct Standard-Model parameter. Their unmeasured numerical values do not imply a missing perturbative class in the calculation. An absolute coefficient still includes the chosen reference-state block; [1] keeps that intercept visible in the total stiffness used in equations (4) and (7).

The full retarded kernel depends on frequency, wave number and the prepared state. Its real and absorptive components contain causal poles, Landau and production continua. The infrared representation used here is the stated simple, underdamped, massless two-helicity branch with no additional unsuppressed long-range scalar. Causal branch selection is a testable property of the full response rather than an inference from a static coefficient [1].

This distinction also organizes the pole analysis. A double zero on a principal logarithmic sheet is an analytic benchmark. Crossing a production cut changes the equation satisfied by a physical damped resonance on the adjacent retarded sheet. The explicit continuation in [1] identifies a simple underdamped resonance in the tested channel, while the separately specified low-energy massless branch supplies the propagating infrared completion. Static slope, sheet-dependent resonance and massless two-helicity wave are consequently three defined response statements.

The macroscopic representative uses a positive fixed density ϖ and an auxiliary symmetric source $q_{\mu\nu}$ with determinant q. Its fixed-measure composite metric is

$$\hat{g}_{\mu\nu}=\left(\frac{\varpi}{\sqrt{-q}}\right)^{1/2} q_{\mu\nu}, \sqrt{-\hat{g}}=\varpi . \quad (6)$$

The density defines a source measure and contributes no independent microscopic metric Hilbert space. Its Weyl redundancy and volume-preserving diffeomorphisms define the chosen Weyl-transverse-diffeomorphism (WTDiff) infrared completion [8, 9]. A real shear with $q_{xy}=q_{yx}=h_k e^{ikz}+h_{-k}e^{-ikz}$ gives a direct normalization test. The completed SM quadratic response is $2A_{2,E}^{tot}V_4 k^2 h_k h_{-k}$. In the fixed-measure curvature action, the symmetric tensor contraction counts both off-diagonal components. Matching these two quadratic forms fixes the WTDiff curvature coefficient C_W and restores dimensions without a natural-unit convention [1, 2]:

$$C_W=2A_{2,E}^{tot}=\frac{\hbar c^5}{16\pi G}, \frac{G}{c^4}=\frac{\hbar c}{32\pi A_{2,E}^{tot}} . \quad (7)$$

Here $\hbar$ is the reduced Planck constant, c the locally realized signal speed and G the long-wavelength Newton coupling. With the complete conserved stress tensor $T_{\mu\nu}$, its trace T, the Ricci tensor $R_{\mu\nu}$ and scalar R of the composite metric, the fixed-measure variation yields

$$R_{\mu\nu}-1/4\,\hat{g}_{\mu\nu}R=\frac{8\pi G}{c^4}\left(T_{\mu\nu}-1/4\,\hat{g}_{\mu\nu}T\right). \quad (8)$$

Stress conservation and the contracted Bianchi identity imply a constant Λ on a connected solution branch and yield the Einstein-form conserved-source equation

$$R_{\mu\nu}-1/2\,\hat{g}_{\mu\nu}R+\Lambda\,\hat{g}_{\mu\nu}=\frac{8\pi G}{c^4}T_{\mu\nu} . \quad (9)$$

The equations reproduce the tested local Einstein dynamics for conserved sources on this infrared branch. Their geometric tensors encode the collective response of matter. The constrained sector of equation (9), together with the radiative TT sector, is essential to the finite-body calculation in Section 6.

3. Homogeneous vacuum shifts leave the local response invariant

A physical vacuum can polarize, fluctuate and respond to boundaries. The identity-operator energy zero is a different object: every state receives the same constant offset. The fixed-measure source makes this difference explicit before any response derivative [1, 3, 10]. Let Φ denote all SM fields, Ω a fixed integration domain and L_{SM} the renormalized Lagrangian coupled through equation (6). Let ρ_0 be a spacetime-independent identity coefficient. Holding the physical preparation, nonidentity couplings, measure, topology and boundary data fixed gives

$$L_{SM} \to L_{SM} - \rho_0, S_{SM} \to S_{SM} - \rho_0 V_\varpi, V_\varpi = \int_\Omega d^4x\, \varpi. \quad (10)$$

The four-volume V_ϖ does not vary with either independent CTP source. Both branches acquire opposite, source-independent phases. Thus the identity holds before the sources coincide:

$$Z'[q_+, q_-] = \exp\left[-\frac{i\rho_0}{\hbar}(V_\varpi - V_\varpi)\right] Z[q_+, q_-] = Z[q_+, q_-]. \quad (11)$$

Every derivative of the connected functional in equation (2) is consequently identical before and after the shift. This includes mean projected stress, separated correlators, local seagull/contact terms, the completed Hessian, fluctuations and higher vertices. The stiffness and matched coefficient chain are therefore invariant under this *common energy-origin operation*. At the infrared level the same result appears in equation (8): a shift of $T_{\mu\nu}$ by $-\rho_0 \hat{g}_{\mu\nu}$ cancels in the trace-free combination [1, 3].

The cosmological constant appearing in equation (9) has the status of an integration datum. Its representative changes when the identity origin changes, while the invariant branch label remains fixed. Write $T_{\mu\nu} = T^{(0)}_{\mu\nu} - \rho_{id}\hat{g}_{\mu\nu}$, where $T^{(0)}_{\mu\nu}$ contains no homogeneous identity term. The invariant datum is

$$\Lambda_{inv} = \Lambda + \frac{8\pi G}{c^4}\rho_{id}. \quad (12)$$

The exact result removes the arbitrary radiative identity term as a *local source* at every order within this fixed-measure matter theory. The invariant datum is independently specified; the theorem does not calculate its measured value. State differences, vacuum polarization, connected fluctuations, phase-transition effects, Casimir and boundary stresses, and anomaly-induced nonidentity terms remain response-bearing. A cosmology on the zero invariant branch is therefore a declared branch choice, examined next, and not a corollary that all vacuum physics has vanished.

The location of the fixed-measure operation matters. With an ordinary variable determinant, the doubled vacuum action is the difference of two integrals of the square root of the respective source determinants. That difference vanishes when the sources coincide, yet its first derivative with respect to their difference need not vanish. The CTP contour alone is therefore insufficient. Equation (6) makes each branch volume independent of its probe source *before* equation (11) is differentiated. Completed local contact terms inherit the same invariance, so no discarded shear seagull reintroduces the identity coefficient. Running curvature operators and trace anomalies remain allowed because their source dependence belongs to nonidentity response [1, 3].

4. An operational reconstruction of cosmic acceleration

The epoch-state hierarchy separates the scale of a bound atom from the space between galaxies without invoking instantaneous long-range coordination. Similar coarse-grained epoch states give similar local fractional rates, while motion, support forces, source-

established ambient response and inhomogeneity provide their own corrections. The hot early universe and subsequent binding thresholds supply the physical preparation in which durable atomic clocks and rulers became possible. The background law applies to that specified bound-state comparison branch; it does not extrapolate one late-time ruler unchanged through every earlier phase [4].

The same response is evaluated on different physical states. An *epoch state* describes the homogeneous coarse-grained background, an *ambient state* adds the response near a localized source, and a body's *prepared state* adds its own loading and internal structure [4]. The common long-distance Green function belongs to the shared ambient branch; an altered compact body does not receive a private gravitational constant [1]. The cosmological comparison concerns the epoch history of stable SM clocks and rulers.

Let $L(t)$ be the length of one specified material ruler at epoch t, $\omega_a(t)$ a specified atomic transition angular frequency, and $A_{2,E}(t)$ the corresponding epoch stiffness on the declared common-scale branch. Let t_0 denote reception today. The matter-standard comparison factor $A(t)$ and its logarithmic rate are [4]

$$A(t)=\frac{L(t_0)}{L(t)}=\frac{\omega_a(t_0)}{\omega_a(t)}=\sqrt{\frac{A_{2,E}(t_0)}{A_{2,E}(t)}},\ H_{op}(t)=\frac{\dot{A}}{A}=-\frac{\dot{L}}{L}. \quad (13)$$

The equalities specify a common-scale state trajectory, with dimensionless transition, composition and protocol effects held fixed or treated separately. They do not result from a coordinate relabelling. Under source-free signal propagation and homogeneous endpoint preparations, comparison of emission and reception gives

$$1+z=\frac{1}{A(t_e)}=\frac{L(t_e)}{L(t_0)}=\sqrt{\frac{A_{2,E}(t_e)}{A_{2,E}(t_0)}},\ H_{op}(z)=-\frac{1}{1+z}\frac{dz}{dt_e}. \quad (14)$$

Here t_e is the emission epoch and z the measured redshift. The signal transports an endpoint comparison rather than accumulating an additional copy of that redshift. The receiver-unit radial distance D_C, transverse comoving distance D_M, Hubble distance D_H and Alcock–Paczyński observable F_{AP} obey the same tested observational relations as the infrared geometric representation [4, 11]:

$$D_C(z)=c_0\int_0^z\frac{dz'}{H_{op}(z')},\ D_H(z)=\frac{c_0}{H_{op}(z)},\ F_{AP}(z)=\frac{D_M(z)}{D_H(z)}. \quad (15)$$

For the spatially flat distance comparison used in the versioned benchmark, $D_M=D_C$. Defining $H_0=H_{op}(t_0)$ and $E(z)=H_{op}(z)/H_0$ then gives $F_{AP}=E(z)\int_0^z dz'/E(z')$. The inverse ruler scale can be called an effective scale factor, but its measured curvature here follows evolving matter standards.

Distance duality follows the same transparent signal and endpoint accounting: angular-diameter distance and luminosity distance are related by two powers of the measured

redshift [11]. A standard spectral transition cannot independently be rescaled at emission and then assigned a second geometric redshift during transport. The local limiting signal speed in equation (15) is expressed in the receiver's units; the response theory distinguishes that propagation rule from the state comparison of equation (14). These definitions make chronometer, distance and Alcock–Paczyński tests mutually compatible within the chosen homogeneous protocol [4].

The time dependence has a conserved energy ledger. Let E_{drive} be the available state inventory sustaining an earlier scale and let $P_{loss} \geq 0$ be the irreversible power that depletes that availability. With entropy production rate $\dot{S}_{prod}$ and a declared reference temperature T_{ref}, the homogeneous thermodynamic account gives [4]

$$H_{op} = \frac{P_{loss}}{E_{drive}} = -1/2 \frac{\dot{A}_{2,E}}{A_{2,E}}, P_{loss} = T_{ref} \dot{S}_{prod}, \tau_{eff} = \frac{E_{drive}}{P_{loss}}. \quad (16)$$

Total energy remains conserved; irreversibility changes the part available to support the former state. The equation identifies a microscopic SM target, including reactions, thresholds, binding, transport and stress correlations. The measured effective time history is reconstructed here from data rather than presented as an independent first-principles prediction.

Let $u = H_0 (t_0 - t)$ be dimensionless lookback, $x = \ln(1+z)$, and $\theta(u) = H_0 \tau_{eff}(t)$. The effective-time equation and normalized expansion law are [4]

$$\frac{du}{dx} = \theta(u), E(z) = \frac{1}{\theta[u(z)]}, \theta(u) = 1 - \alpha u - 1/2 \beta u^2. \quad (17)$$

The dimensionless coefficients α and β describe the slope and curvature of the lowest-order effective-time law that admits an acceleration turnover. The self-similar limit has $E(z) = 1+z$. Define the residual entropy/availability response $R_{ent}(z) = E(z)/(1+z)$. The observational deceleration identity becomes [4]

$$q_{op}(z) = \frac{d \ln R_{ent}}{d \ln(1+z)} = -1 + \alpha + \beta u(z). \quad (18)$$

Thus the canonical common-scale stiffness relation fixes the leading scale weight while the reconstructed residual supplies the curvature. A negative present q_{op} is compatible with a continuously contracting material ruler. The zero invariant cosmological branch is chosen in this particular construction; a physical dark-energy fluid does not enter equations (13)–(18).

At a fixed $H_0 = 69\, km\, s^{-1} Mpc^{-1}$, the 32-chronometer diagonal-error fit in the versioned v0.3 numerical package gives $\alpha = 0.510 \pm 0.186$, $\beta = 1.103 \pm 0.552$, a coefficient correlation of -0.962, and $\chi^2 = 11.84$ for 30 degrees of freedom [4, 12]. It gives $q_{op}(0) = -0.490 \pm 0.186$ and a turnover at $z = 0.70^{+0.32}_{-0.14}$, with the latter interval propagated using the correlated parameter covariance. Fig. 2 displays the fitted chronometer history and the self-similar and conventional flat-ΛCDM references.

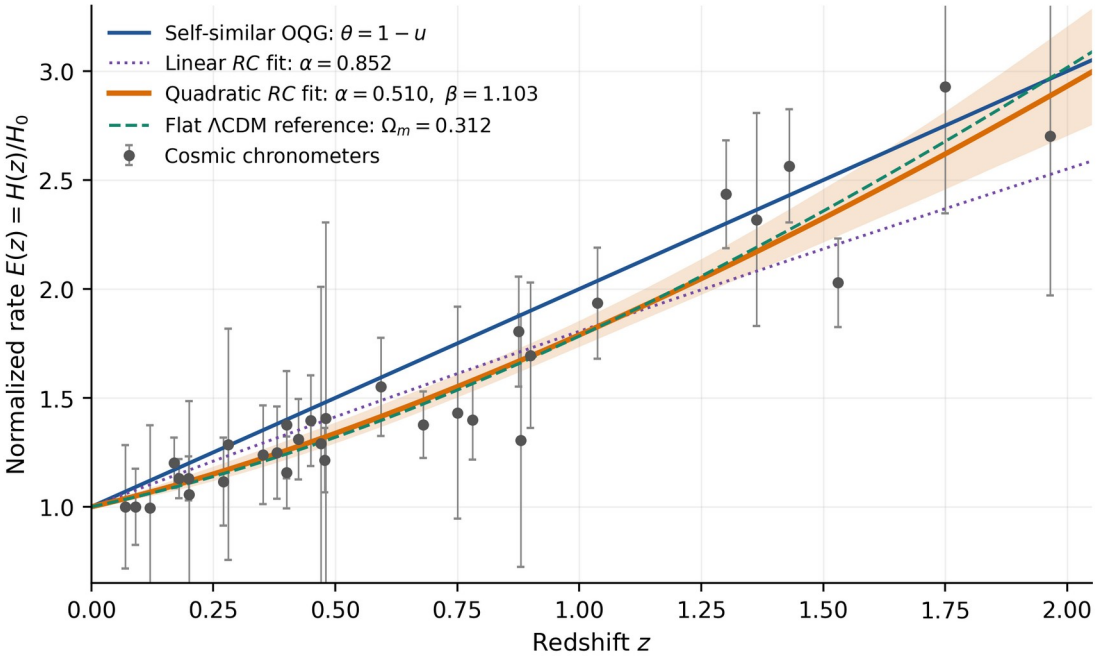


Fig. 2. The versioned v0.3 chronometer fit, with displayed diagonal errors and a fixed present Hubble datum. The quadratic law is a two-parameter background reconstruction [4].

The six DESI DR2 F_{AP} values were then evaluated with these chronometer-fit coefficients and no DESI refit [4, 13]. The quadratic law gives a diagonal-error statistic of 6.60 for those six points; the one-parameter flat-ΛCDM reference fitted to the same chronometers gives 6.55. All six marginal residuals of the quadratic law are below 1.55 displayed standard deviations. Fig. 3 gives the corresponding no-refit comparison. The law was selected after high-redshift behavior had been inspected, and these statistics use displayed diagonal errors. They establish a feasible background reconstruction and a cross-dataset consistency check; a covariance-complete likelihood, early-time and structure observables, and the calculated microscopic epoch relaxation test its reach.

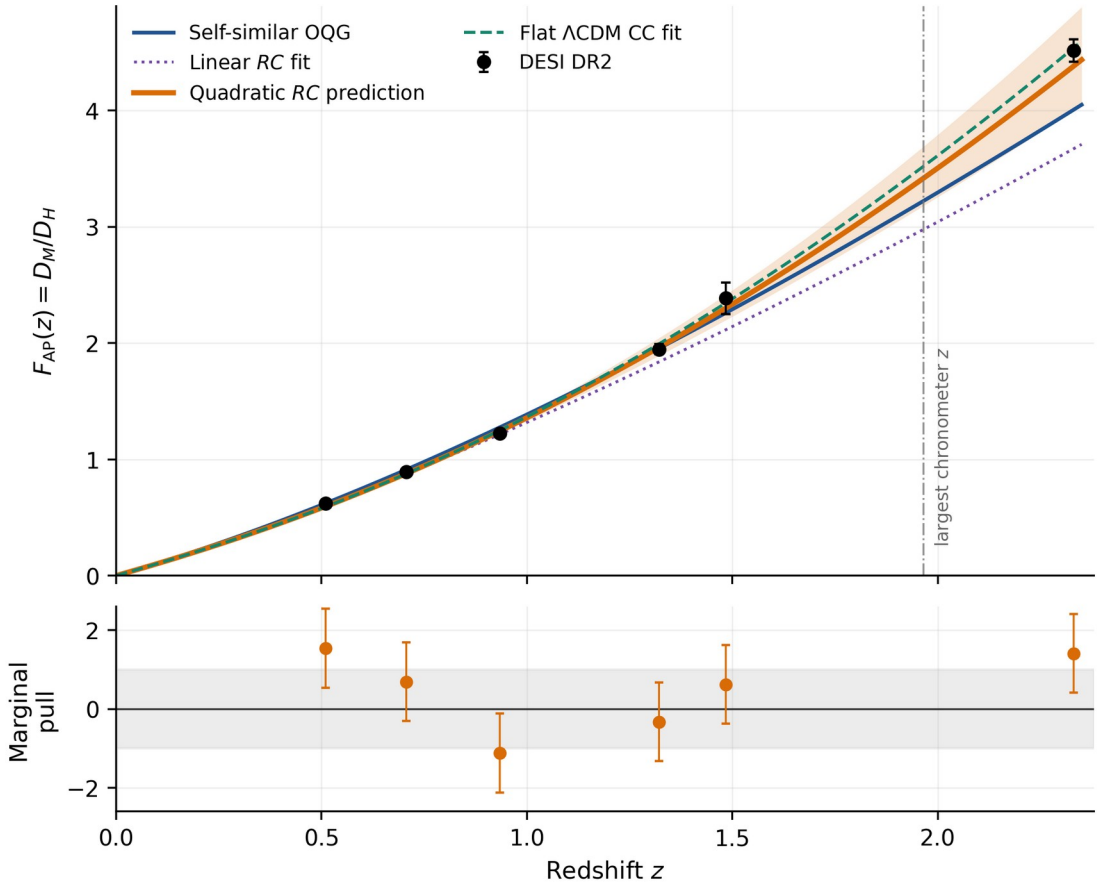


Fig. 3. Six DESI DR2 Alcock–Paczyński values and marginal residuals. The response parameters are from chronometers alone; the highest-redshift point extends modestly beyond the chronometer range [4, 13].

The conventional flat cosmological reference in Fig. 2 is a one-parameter model fitted to the *same* chronometer set. It is a comparison curve, rather than an external constraint on the OQG fit. Planck's parameter analysis supplies the broader conventional cosmological baseline [14]. The OQG numerical archive retains every input row, parameter covariance, six no-refit predictions and source grids for the figures. Its statistics are descriptive diagonal-error diagnostics, which permits reproduction of the quoted arithmetic while leaving joint covariance and early-universe model selection to further observational tests [4].

5. Positive material extension through collapse

In the geometric account, singularity theorems identify incomplete causal geodesics under their hypotheses [15]. The material question posed here is narrower and operational: whether a resolved quantum state of the collapsing system becomes an exact point with zero internal extension. The geometric conclusion and the material conclusion use different state spaces, so the latter requires a direct quantum argument.

Black-hole interpretation asks whether a derived geometric endpoint also ends a material quantum state. The relevant theorem concerns a regular resolved sector of matter, such as center-relative collective displacements of an extended body, and states its continuation gate explicitly [5]. Let $\hat{X}$ be one position-like internal observable and $\hat{P}$ its conjugate, with $[\hat{X},\hat{P}]=i\hbar\hat{I}$. Let $L_{op}>0$ denote a root-mean-square extension in a reference normal state, and let $b=L_{op}(\rho)/L_{op}(\rho_0)$ be its dimensionless relative scale. Set $\chi=-\ln b$. Finite scaling of the resolved pair has the reciprocal form

$$\hat{X}\mapsto b\,\hat{X},\ \hat{P}\mapsto b^{-1}\hat{P},\ b=e^{-\chi}>0. \quad (19)$$

The commutator, symplectic form, complete Robertson–Schrödinger uncertainty matrix and state norm are preserved for every finite χ. The symmetric dilation generator $\hat{D}=(\hat{X}\hat{P}+\hat{P}\hat{X})/2$ has a finite unitary implementation $U(\chi)=\exp(i\chi\hat{D}/\hbar)$ in the regular sector [5]. This unitary scale map is a comparison of states, not a claim that a collapsing star evolves solely by that operator.

Let ρ be a normal, trace-one state with finite second moments and let its selected continuous position-like observable have no normalizable exact-zero eigenstate. Its center-relative mean-square coordinate is $Tr(\rho\hat{X}^2)>0$. For finitely many resolved coordinates $\hat{X}_j$, positive weights w_j give an extension

$$L_{op}^2(\rho)=\sum_j w_j\,Tr(\rho\hat{X}_j^2)>0. \quad (20)$$

The positivity follows directly from the spectral measure: a zero integral of a nonnegative squared coordinate would require unit probability at exact zero, whereas the zero-eigenvalue projector vanishes. Mixed normal states obey the same proof. An arbitrarily narrow *positive* state remains permitted; no universal minimum length follows. Exact zero is the boundary $\chi\to+\infty$, where the reciprocal momentum scaling has no inverse and the limit is not a normal state in the declared sector [5].

A dynamical statement additionally uses a cumulative finite-loading label λ. If the logarithmic response is absolutely continuous and its total magnitude is integrable on every finite loading interval, then

$$\chi(\lambda)=\chi(0)+\int_0^{\lambda}\frac{d\chi}{d\lambda'}d\lambda',\ \int_0^{\lambda_f}\left|\frac{d\chi}{d\lambda'}\right|d\lambda'<\infty\,(\lambda_f<\infty)\Rightarrow b(\lambda_f)>0. \quad (21)$$

Equation (21) is the finite-loading corollary. With an available regular branch at each finite stage, matter passes through successively positive extensions even if its limit tends to zero. Horizons remain possible one-way causal boundaries in the emergent representation. A terminating geodesic of that representation and an exact zero-extension material state are different claims. The theorem excludes the latter on the declared sector and tests the former's physical interpretation [5]. Its own gate is concrete: a strong-field calculation of the state-dependent scale susceptibility, including phase changes and any change of canonical chart, determines whether the integrability and branch conditions persist. The

result identifies the admissible endpoint without postulating a bounce, remnant or smallest radius.

The no-zero result is stronger than observing that the scale map fails at zero. Even if an exact endpoint were appended by hand, its proposed mean-square extension would require a probability measure concentrated at the exact zero eigenvalue of a continuous position-like observable. That projector vanishes by the theorem's explicit coordinate premise. A sequence of normalized packets may concentrate in its coordinate *probability distributions* while having no normalized strong Hilbert-space limit. This is the precise sense in which zero is an approached boundary and never one more finite state [5].

6. A coherent gravitational entangling phase without a bridge

Two finite bodies in spatial superposition provide a final operational test. Each body's left and right paths form a two-level *path qubit*: a coherent pair of alternatives, with no additional hardware implied. The mass m_1 belongs to body 1 and m_2 to body 2. For a quasistatic hold time τ, let r_{ij} be the separation between path i of the first body and path j of the second, where each index is left or right. The constrained conserved-source limit of equation (9), with the common ambient G, supplies the leading interaction energy and phase [1, 6, 7]:

$$U_{ij} = -\frac{G m_1 m_2}{r_{ij}}, \phi_{ij} = -\frac{1}{\hbar}\int_0^\tau U_{ij}\, dt = \frac{G m_1 m_2 \tau}{\hbar r_{ij}}. \quad (22)$$

For finite bodies the reciprocal separation is replaced by the double integral over their normalized branch mass profiles [1]. The same constrained source law supplies all four branch energies. The radiative TT block alone cannot substitute for this source completion.

If $f_{1,i}(x)$ and $f_{2,j}(y)$ are normalized spatial mass profiles of the two bodies on branches i, j, the finite-size replacement is

$$\frac{1}{r_{ij}} \to \int d^3x\, d^3y \frac{f_{1,i}(x) f_{2,j}(y)}{|x-y)}. \quad (23)$$

Time-dependent paths require the corresponding integral over their actual hold, splitting and recombination histories. This explicitly ties the phase to an apparatus specification rather than assuming point masses at fixed positions for every protocol.

Independent phases assigned to one body can be removed locally. The alternating combination cancels those one-body phases and leaves the invariant joint phase Φ. For initially equal independent path superpositions with negligible visibility loss, the pure-state concurrence C is [1]

$$\Phi = \phi_{LL} + \phi_{RR} - \phi_{LR} - \phi_{RL}, C = \left|\sin(\Phi/2)\right|. \quad (24)$$

The conserved-source WTDiff completion fixes the same coherent infrared phases as an Einstein-equivalent account on the declared branch. This is an operational equivalence of the measured coherent phase, not a statement that their microscopic descriptions coincide.

The normalized SM response involves noncommuting stress operators and contains fluctuations and higher connected responses. For probe histories a, b, an off-diagonal reduced-state element separates its coherent phase Θ_{ab} from visibility loss $\Gamma_{ab} \geq 0$:

$$\rho_{ab}(t_f) = \rho_{ab}(t_i) \exp(i\Theta_{ab} - \Gamma_{ab}). \quad (25)$$

The retarded compliance fixes the coherent term. The symmetrized fluctuation kernel of the prepared laboratory state fixes the visibility exponent. Equality of the mean and retarded responses on a tested source domain gives the same coherent phase through second order; equality of a full Gaussian reduced map also requires equality of its noise kernel [1]. This makes retardation, correlated noise and higher connected stress response useful discriminators beyond a static phase.

A certified entanglement witness, under the protocol's locality and subsystem assumptions and after nongravitational channels have been controlled, establishes a nonclassical effective interaction channel [6, 7, 16–18]. Equation (24) has a matter-response realization with no separately fundamental metric subsystem. Thus a literal ER tunnel is absent from the OQG construction and is unnecessary for this EPR application. A static witness does not establish a mathematical prohibition on every effective wormhole representation; its direct result is the nonclassical phase of the tested matter channel.

7. Joint consistency and conclusion

One normalized SM source supports four different, checkable statements. The exact identity-shift theorem acts before differentiation and protects local response from an arbitrary radiative energy origin. The epoch-state map makes the same response measurable as a matter-standard cosmological history; on the selected zero invariant branch, the fitted background acceleration needs no physical dark-energy fluid. Regular finite canonical scaling has no exact zero-extension normal endpoint, with a precise integrability gate for finite-loading continuation. The Einstein-equivalent conserved-source sector fixes the four-branch coherent BMV phase without a fundamental bridge.

The consistency conditions cross sections. The vacuum theorem leaves a global invariant branch datum and physical state differences available for cosmology. Epoch stiffness belongs to a common background, whereas a compact prepared body changes a local operator within a shared ambient response. The collapse theorem uses an actual canonical state transformation rather than a change of coordinates. The finite-body phase uses the constrained conserved-source exchange rather than radiative TT modes alone. The causal two-helicity branch links the static coefficient to an infrared representative while keeping its Lorentzian tests explicit.

The numerical high-state coefficient ledger has three independently defined inputs: the Higgs–curvature coupling and two Yang–Mills lattice observables. The absolute reference-state stiffness is a separately declared normalization datum. Tests of the cosmological time law, branch survival at high density and apparatus-specific noise sharpen the four outcomes without changing what has been proved at their stated scopes. In that sense OQG gives four operational forms to apparent spacetime problems while retaining the

successful Einstein-equivalent comparison equations. Matter tells matter how to scale. Geometry is bookkeeping for the comparison.

Acknowledgements and declarations

This work was self-funded. The author declares no conflict of interest. An overview of OQG was presented at the Alternative Propulsion Engineering Conference on 19 September 2026; this four-result synthesis was prepared afterward. The author used OpenAI ChatGPT and Codex for literature organization, calculation cross-checks, manuscript assembly and editing, and reviewed the resulting scientific claims and text. The cosmology inputs, code, verification outputs and original figures are contained in the versioned OQG in Practice v0.3 numerical reproducibility package described in [4]. The v0.3 complete-derivation manuscript [1] supplies the detailed perturbative coefficient ledger and numerical checks.

References

[1] T.J. Desiato, “Operational Quantum Gravity: From Standard Model Stress Response to Gravity-Induced Entanglement”, complete derivation draft v0.3, 17 September 2026, unpublished manuscript.

[2] T.J. Desiato, “OQG Hessian to WTDiff Einstein Companion”, v0.3, 12 September 2026, unpublished manuscript.

[3] T.J. Desiato, “Operational Quantum Gravity Prevents the Vacuum Catastrophe”, v0.3, 12 September 2026, unpublished manuscript.

[4] T.J. Desiato, “Operational Quantum Gravity in Practice: Spectral Stiffness, Matter Scaling, Equivalence, and Cosmology without Dark Energy”, v0.3, 5 September 2026, unpublished manuscript and associated v0.3 numerical reproducibility package.

[5] T.J. Desiato, “OQG Canonical Scale Zero Extension”, v0.3, 6 September 2026, unpublished manuscript.

[6] S. Bose et al., “Spin entanglement witness for quantum gravity”, *Physical Review Letters*, **119**, 240401, 2017. DOI: 10.1103/PhysRevLett.119.240401.

[7] C. Marletto and V. Vedral, “Gravitationally induced entanglement between two massive particles is sufficient evidence of quantum effects in gravity”, *Physical Review Letters*, **119**, 240402, 2017. DOI: 10.1103/PhysRevLett.119.240402.

[8] E. Álvarez, D. Blas, J. Garriga and E. Verdaguer, “Transverse Fierz-Pauli symmetry”, *Nuclear Physics B*, **756**, pp. 148–170, 2006. DOI: 10.1016/j.nuclphysb.2006.08.003.

[9] E. Álvarez and R. Vidal, “Weyl transverse gravity and the cosmological constant”, *Physical Review D*, **81**, 084057, 2010. DOI: 10.1103/PhysRevD.81.084057.

[10] R. Carballo-Rubio, “Longitudinal diffeomorphisms obstruct the protection of vacuum energy”, *Physical Review D*, **91**, 124071, 2015. DOI: 10.1103/PhysRevD.91.124071.

[11] I.M.H. Etherington, “On the definition of distance in general relativity”, *Philosophical Magazine*, **15**, pp. 761–773, 1933. DOI: 10.1080/14786443309462220.

[12] A. Favale, A. Gómez-Valent and M. Migliaccio, “Cosmic chronometers to calibrate the ladders and measure the curvature of the Universe”, *Monthly Notices of the Royal Astronomical Society*, **523**, pp. 3406–3422, 2023. DOI: 10.1093/mnras/stad1621.

[13] DESI Collaboration, “DESI DR2 results II: Measurements of baryon acoustic oscillations and cosmological constraints”, *Physical Review D*, **112**, 083515, 2025. DOI: 10.1103/tr6y-kpc6.

[14] Planck Collaboration, “Planck 2018 results. VI. Cosmological parameters”, *Astronomy & Astrophysics*, **641**, A6, 2020. DOI: 10.1051/0004-6361/201833910.

[15] R. Penrose, “Gravitational collapse and space-time singularities”, *Physical Review Letters*, **14**, pp. 57–59, 1965. DOI: 10.1103/PhysRevLett.14.57.

[16] M. Christodoulou et al., “Locally mediated entanglement in linearized quantum gravity”, *Physical Review Letters*, **130**, 100202, 2023. DOI: 10.1103/PhysRevLett.130.100202.

[17] D.L. Danielson, G. Satishchandran and R.M. Wald, “Gravitationally mediated entanglement: Newtonian field versus gravitons”, *Physical Review D*, **105**, 086001, 2022. DOI: 10.1103/PhysRevD.105.086001.

[18] E. Martín-Martínez and T.R. Perche, “What gravity mediated entanglement can really tell us about quantum gravity”, *Physical Review D*, **108**, L101702, 2023. DOI: 10.1103/PhysRevD.108.L101702.